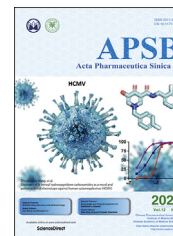




Chinese Pharmaceutical Association
Institute of Materia Medica, Chinese Academy of Medical Sciences

Acta Pharmaceutica Sinica B

www.elsevier.com/locate/apsb
www.sciencedirect.com



ORIGINAL ARTICLE

Milk-derived exosomes exhibit versatile effects for improved oral drug delivery



Lei Wu^{a,†}, Lingling Wang^{a,†}, Xi Liu^a, Yuli Bai^a, Ruinan Wu^a,
Xiang Li^a, Yutong Mao^a, Ling Zhang^b, Yongxiang Zheng^c, Tao Gong^a,
Zhirong Zhang^a, Yuan Huang^{a,*}

^aKey Laboratory of Drug Targeting and Drug Delivery System, Ministry of Education, West China School of Pharmacy, Sichuan University, Chengdu 610041, China

^bSichuan University, College of Polymer Science and Engineering, Chengdu 610041, China

^cSichuan University West China School of Pharmacy, Chengdu 610041, China

Received 19 August 2021; received in revised form 9 November 2021; accepted 20 December 2021

KEY WORDS

Milk-derived exosomes;
Oral drug delivery system;
Apical-to-basolateral transport;
pH Adaptation;
Biomimetic vehicles;
Insulin;
Transcytosis;
Signal regulation

Abstract As endogenous courier vesicles, exosomes play crucial roles in macromolecule transmission and intercellular communication. Therefore, exosomes have drawn increasing attention as biomimetic drug-delivery vehicles over the past few years. However, few studies have investigated the encapsulation of peptide/protein drugs into exosomes for oral administration. Additionally, the mechanisms underlying their biomimetic properties as oral delivery vehicles remain unknown. Herein, insulin-loaded milk-derived exosomes (EXO@INS) were fabricated and the *in vivo* hypoglycemic effect was investigated on type I diabetic rats. Surprisingly, EXO@INS (50 and 30 IU/kg) elicited a more superior and more sustained hypoglycemic effect compared with that obtained with subcutaneously injected insulin. Further mechanism studies indicated that the origin of excellent oral-performance of milk-derived exosomes combined active multi-targeting uptake, pH adaptation during gastrointestinal transit, nutrient assimilation related ERK1/2 and p38 MAPK signal pathway activation and intestinal mucus penetration. This study provides the first demonstration that multi-functional milk-derived exosomes offer solutions to many of the challenges arising from oral drug delivery and thus provide new insights into developing naturally-equipped nanovehicles for oral drug administration.

© 2022 Chinese Pharmaceutical Association and Institute of Materia Medica, Chinese Academy of Medical Sciences. Production and hosting by Elsevier B.V. This is an open access article under the CC BY-NC-ND license (<http://creativecommons.org/licenses/by-nc-nd/4.0/>).

*Corresponding author.

E-mail address: huangyuan0@163.com (Yuan Huang).

[†]These authors made equal contributions to this work.

Peer review under responsibility of Chinese Pharmaceutical Association and Institute of Materia Medica, Chinese Academy of Medical Sciences.

<https://doi.org/10.1016/j.apsb.2021.12.015>

2211-3835 © 2022 Chinese Pharmaceutical Association and Institute of Materia Medica, Chinese Academy of Medical Sciences. Production and hosting by Elsevier B.V. This is an open access article under the CC BY-NC-ND license (<http://creativecommons.org/licenses/by-nc-nd/4.0/>).

1. Introduction

In the past decades, biologicals have achieved tremendous breakthroughs in the treatment of various diseases¹, and numerous novel delivery strategies have been developed to overcome administration dilemma such as degradation susceptibility, immunogenicity and physiological absorption barriers². Exosomes, which are considered as natural cell-secreted “Trojan Horse”, encapsulate endogenous functionally active macromolecules (such as DNA, miRNA, mRNA and proteins) and can efficiently deliver these cargoes to recipient cells, to enable cell-to-cell communication³. Due to their advantages such as high biocompatibility, long circulating time and intrinsic ability to encapsulate biological macromolecules, exosomes have drawn increasing attention as novel biologics-delivery vehicles^{4–6}. However, the practical application of exosome-based therapeutics in clinical transformation remains an ongoing challenge. Many studies isolated exosomes from cell culture media with a low yield and a high cost, which makes scaled-up production difficult⁴. Based on the current limitations, a cost-effective and scalable source should be optimized.

It was reported that bovine milk-derived exosomes (EXOs) exhibited similar potential to serve as drug delivery nanocarriers⁷. On the other hand, milk is a more affordable and accessible source compared to cell culture media. Moreover, EXOs might provide additional benefits as naturally desirable oral delivery carriers, which indicates that EXOs constitute a more convenient and patient-friendly therapeutic modality⁵. The anatomy of the gastrointestinal tract (GIT) poses significant challenges to oral macromolecules delivery^{8,9}. However, it was reported that nucleic acids encapsulated in EXOs could be delivered orally into the bloodstream in bioactive form¹⁰, but the potential to deliver biomacromolecular drugs such as peptide/protein drugs and the origin of good oral-performances of EXOs remains elusive¹¹. Insights into how natural nanocarriers traverse GIT might provide information that aids the development of oral vehicles.

To investigate the potential of EXOs to serve as natural protein delivery vehicles, insulin (INS)-loaded milk-derived exosomes (EXO@INS) was fabricated in the present study and the *in vivo* hypoglycemic effect was investigated on type I diabetic rats. Surprisingly, EXO@INS elicited a more excellent and sustained hypoglycemic effect compared with that obtained with subcutaneously injected INS, indicating the superior oral bioavailability of EXOs. And then we investigated biomimetic principles as an oral vehicle in terms of EXOs-cell interaction. On one hand, the ability of nanocarriers to overcome oral delivery barriers in the GIT was investigated. On the other hand, cellular response triggered by EXOs was studied to further clarify the underlying mechanisms.

2. Materials and methods

2.1. Materials

Porcine insulin (INS, 28.2 IU/mg) was purchased from Wanbang Bio-Chemical Co., Ltd. (Jiangsu, China). Fluorescein isothiocyanate (FITC) was obtained from J&K Scientific Ltd. (Beijing, China). Gly-Sar was bought from TCI (Tokyo, Japan). 1,1'-Dioctadecyl-3,3,3',3'-tetramethylindocarbocyanine perchlorate (DiI) was purchased from Invitrogen (Carlsbad, CA, USA). Lysosome Tracker Red and GA Tracker Red were obtained from Beyotime Biotechnology (Shanghai, China). ER Tracker Green was bought

from Key GEN Biotech Corp. (Jiangsu, China). All other chemicals were purchased from Sigma–Aldrich (St. Louis, MO, USA) and Shanghai Chemical Reagents Co. (Shanghai, China) and used as received, unless otherwise stated.

2.2. Isolation of milk-derived exosomes

Low fat bovine milk was purchased in a grocery store. Milk was centrifuged at 13,000×g for 30 min at 4 °C to remove somatic cells and debris¹². The supernatant and EDTA (pH 7.0, 500 mol/L) were mixed (3:1, v/v) on ice for 15 min to precipitate milk casein. The suspension was ultracentrifuged at 100,000×g (Beckman Coulter, SW41Ti rotor, Brea, CA, USA) for 60 min (4 °C) to remove fat globules, precipitated protein and larger vesicles. The supernatant was ultracentrifuged at 135,000×g (Beckman Coulter, SW41Ti rotor, Brea, CA, USA) for 90 min (4 °C) to isolate exosomes. The exosome pellets were resuspended in PBS. The total protein concentration was measured by BCA kit. Then, EXOs (<6 mg/mL) were stored at –80 °C until use.

2.3. Preparation of insulin-loaded exosomes

EXOs (1 mg/mL) and insulin (INS) (8 mg/mL) were mixed followed by sonication (100 W, 3 min, 2 s/2 s on/off). The unloaded INS was removed by ultrafiltration (MWCO: 100 kDa). The structure of EXO@INS was destroyed by adding 1% Triton X-100 (1:1, v/v) and the content of loaded INS was quantified by high-performance liquid chromatography (HPLC)¹³. The drug loading of EXO@INS was calculated according to Eqs. (1) and (2)¹⁴:

$$\text{Drug loading (\%)} = W_{\text{INS}}/W_{\text{TOTAL}} \times 100 \quad (1)$$

$$\text{Encapsulation efficiency (\%)} = W_{\text{INS}}/W_{\text{ALL}} \times 100 \quad (2)$$

where W_{INS} is the weight of loaded INS, W_{TOTAL} is the total weight of exosomal protein and loaded INS, and W_{ALL} is the total weight of feed INS.

2.4. Characterization of exosomes and insulin-loaded exosomes

Dynamic Light Scattering (DLS) size and zeta potential were measured by Zetasizer Nano ZS90 (Malvern Instruments Ltd., UK). Nanoparticle-tracking analysis (NTA) was performed using Nanosight LM10 (Malvern Instruments Ltd., UK). TEM analysis was carried out as previously described¹⁵. EXOs and EXO@INS were stained with phosphotungstic acid (2%) for 3 min before observation. The gel electrophoresis and Coomassie staining experiments to detect the protein composition were performed as previously reported¹⁶. The exosomal protein of high and low concentration group was 80 and 56 µg, respectively. The exosomal marker protein CD63, CD81 and TSG101 were detected according to the instructions. Trypan blue quenching experiment was performed to confirm the location of loaded insulin. EXO@FITC-INS, free FITC-INS and EXO/FITC-INS physical mixture were incubated with trypan blue solution (33 µg/mL in 0.1 mol/mL citrate buffer, pH 4.4) for 1 min in 96-well plate. The fluorescence of each sample was measured and expressed as a percentage of the fluorescence of the respective control sample. The INS release and enzymatic stability experiments were performed as reported^{15,17}. The content of INS was measured by HPLC¹⁸. To evaluate the bioactivity of INS, released INS (2 IU/kg) from EXO@INS was collected and subcutaneously injected in mice. Then, blood

glucose was measured by a glucose meter (JPS-6, Yicheng, Beijing, China).

2.5. *In vivo pharmacological and pharmacokinetic studies*

Male Sprague–Dawley rats (190–210 g) were rendered diabetic by intraperitoneal injection of streptozotocin (STZ) at a dose of 70 mg/kg¹⁶. One week after STZ-treatment, rats were considered diabetic when the fasting glycemia was over 16.0 mmol/L. Prior to experiments, rats were fasted overnight but with free access to water. Free INS solution (1 IU/kg, s.c.) was the positive control. The oral administration groups included saline solution, free INS solution (50 IU/kg), INS-free EXOs, EXO@INS (50 IU/kg), EXO@INS (30 IU/kg) and EXO@INS (18 IU/kg). Blood samples were collected from tail veins, and BGL was measured *via* a glucose meter (JPS-6, Yicheng, Beijing, China). To quantify plasma INS concentration, blood samples were centrifuged (3000 rpm, 3 min), and INS was then detected using a porcine insulin ELISA kit (Wuhan ColorfulGene Biological Technology Co., Ltd.). AUC of INS concentration, Fr% and PA% were then calculated according to previous reports^{18,19}. All animals received care in compliance with relevant laws and guidelines outlined in the Guide for the Care and Use of Laboratory Animals. All procedures were approved by Sichuan University Animal Care and Use Committee.

2.6. *Cellular uptake and endocytic mechanisms*

The preparation and characterization of dye-labelled PEG coated poly (lactic-co-glycolic acid) (PLGA)-based nanoparticles (PPNs) were described in the [Supporting Information](#). DiI release profile in PBS was studied to prove the feasibility of DiI-based quantitative and qualitative studies ([Supporting Information Fig. S1](#)). E12 cells were used as mucus-secreting epithelial cell model. PPNs and EXOs were incubated with E12 cells for 3 h. Then, cells were washed with 3% (*v/v*) formalin solution in PBS as previously described above²⁰. 100 μ L of DMSO was added to destroy cells. The fluorescence intensity was detected by a Varioskan Flash Multimode Reader (Thermo Fisher Scientific). The number of cells was corrected by Alamar Blue assay as previously reported²¹. In Caco-2 cells, the process was similar as described above. For endocytic mechanisms studies, Caco-2 cells were incubated with different inhibitors for 30 min prior to the administration of EXOs. Then, cells were incubated with EXOs and inhibitors for another 3 h. The quantification of cellular uptake was same as described above. For TEM analysis, cells were incubated with EXOs for 2 h. After washing thrice with PBS, cells were trypsinized and collected by centrifugation (1000 rpm, 5 min). 0.5% glutaraldehyde was carefully added and cells were resuspended. After 10 min at 4 °C, the cells were collected after centrifugation (12,000 rpm \times 10 min). Then, 3% glutaraldehyde was added and cells were stored at 4 °C. Cells were post-fixed in osmium tetroxide (1%), dehydrated in graded acetone and embedded in araldite as previously described¹⁶. The grids were examined using an electron microscope (JEM-1400PLUS, Japan) at 80 kV.

2.7. *The pH adaptation function of EXOs*

Laurdan generalized polarization (GP) index studies and Young's modulus investigation were described in the [Supporting Information](#). For colocalization study, cells were incubated with EXOs

for 2 h and washed thrice with PBS. Lysosome Tracker was incubated with cells according to the instructions. The nucleus was stained with DAPI for 5 min. The Rr was calculated using Image Pro Plus. For quantitative study, cells were first incubated with EXO@DiI for 2 h, and then treated with specific inhibitors (PBS solution) for another 2 h. The concentrations of these inhibitors were listed as follows. Chloroquine was 150 μ mol/mL and LY294002 was 1 mmol/mL. Next, cells were washed with fresh PBS, and cell associated fluorescence intensity was determined as described above, which reflected the relative cellular retention of EXO@DiI. Hemolysis assay was performed to investigate the pH-sensitive endosomal escape of EXOs, PPNs and HA2 solution. RBCs collected from rats were diluted 1:50 (*v/v*) in PBS of various pH values (7.4, 6.5 and 5.5). Then, RBCs and samples were mixed and incubated for 2 h (37 °C). The UV absorption of supernatant was detected at 540 nm. 1% Triton X-100 was the positive control group, and used as the reference for 100%. EXO@INS collected from the basolateral side of Transwell and the serosa side of detached intestine were analyzed by TEM. Cellular uptake and exocytosis under different pH were performed as previously described, and the concentration of HSA was 80 μ g/mL.

2.8. *ERK1/2 and p38 MAPK signaling pathway investigation*

Transepithelial transport studies were described in the [Supporting Information](#). Exocytosis efficiency investigation was similar to the process of intracellular trafficking study in addition to replacing specific inhibitors with different concentrations of insulin, SB20219 (10 μ mol/mL), U0126 (10 μ mol/mL), monensin (33 μ g/mL) and brefeldin A (25 μ g/mL). For western blot analysis, the total proteins of Caco-2 cells were lysed in RIPA buffer (150 mmol/L NaCl, 1% Triton X-100, 0.5% sodium deoxycholate, 0.1% SDS, 50 μ mol/mL Tris-HCl at pH 7.4, plus a protease inhibitor cocktail). Protein concentrations were detected using a BCA Protein Assay Kit. Equal amounts of proteins (20 μ g) were electrophoresed on SDS polyacrylamide gels. The following procedures were performed as previously describe²².

2.9. *Intestinal distribution and mucus permeability assay*

The preparation and characterization of dye-labelled mucoadhesive nanoparticles (MAPs) were described in the [Supporting Information](#). For *in vivo* intestinal mucus-distribution, EXO@DiI, DiI-loaded PPNs, DiI-loaded MAPs and free DiI were orally administered to male C57BL/6 J mice (18–22 g). After 2 h, mice were sacrificed and the small intestines were removed. The tissues were washed with fresh stimulated intestinal fluid (SIF), opened longitudinally, flattened between two glass slides and observed using confocal fluorescence microscope (Zeiss LSM 800). The coverage (%) was calculated using Image-Pro Plus. To evaluate *in vitro* mucus-permeability, Transwell permeable supports were used. 100 μ g/mL of porcine intestinal mucus was added on the membrane. EXO@DiI, PPNs and MAPs were carefully added onto the mucus. After 2 h, the accumulative permeated amount of DiI was detected. For mucus-staining in E12 cells, rhodamine-conjugated ulexeuropaeus agglutinin I lectin was co-incubated with cells for 10 min, followed by washing with fresh PBS for three times. For nucleus staining, cells were incubated with 4',6-diamidino-2-phenylindole (DAPI) for 5 min. To remove the mucus after internalization, 3% (*v/v*) formalin solution in PBS was used to wash cells for three times.

2.10. Safety evaluations

The *in vitro* cell viability study was performed via Alamar Blue assay as reported²³. The LDH release was detected by the LDH kit (Beyotime Biotechnology, Shanghai, China). Hemolysis assay was carried out using rat RBCs. Prior to the detection, cells were incubated with EXOs (25–250 µg/mL) for 3 h, respectively. To evaluate the *in vivo* toxicity, ICR mice (male, 6–8 weeks) consecutively received once-daily oral doses of EXOs (0.5, 1 and 2 mg/kg) for seven days. The body weight of mice was daily monitored. After the whole administration, mice were sacrificed and blood was collected for the detection of ALT, ALP, AST, ALB and TP. The hematology analysis and Hematoxylin and Eosin (H&E) staining was performed as previously described²⁴.

2.11. Statistical analysis

All data are indicated as means ± SD ($n = 3$), unless otherwise stated. The one-tailed Student's *t*-test and two-tailed Student's *t*-test were performed to compare the two groups. Significant differences were defined with $P < 0.05$ and high significance at $P < 0.01$.

3. Results and discussions

3.1. Isolation and characterization of bovine milk-derived exosomes

Exosomes are small extracellular vesicles with diameters between 30 and 150 nm. In this study, EXOs were isolated using a classical ultracentrifugation method as previously reported¹². The average sizes measured by dynamic light scattering (DLS) and nanoparticle-tracking analysis (NTA) were 72.9 and 83.2 nm, respectively (Fig. 1A and B). The polydispersity index (PDI) was 0.225. The yield of EXOs was 7.24×10^9 particles/mL, which was nearly four times more than that of Caco-2 cells-derived exosomes²⁵. Transmission electron microscopy (TEM) showed round and cup-shaped EXOs with diameters of approximately 100 nm (Fig. 1C). The zeta potential of EXOs in phosphate buffer solution (PBS, pH = 7.4) was -9.8 mV. Western blot analyses demonstrated the existence of exosomal marker proteins CD63, CD81 and TSG101 (Supporting Information Fig. S2). Together, these results indicated the successful isolation of EXOs.

The obtained EXOs were stored in aliquots at -80 °C²⁶, and 7 weeks of storage had no obvious effect on their particle size, zeta potential and protein amount (Fig. 1D and Supporting Information Fig. S3A and S3C). For short-term storage at 4 °C, EXOs were stable up to 7 days (Fig. 1E and Fig. S3B). As shown in Fig. 1F, the size of EXOs did not significantly change in simulated gastric fluid (SGF), simulated intestinal fluid (SIF) and PBS (pH = 7.4) during 8 h-incubation (37 °C). Due to their potential for cost-effective production and long-term storage, EXOs might be promising orally delivered vehicles.

3.2. Preparation and characterization of insulin-loaded milk-derived exosomes

EXOs could encapsulate hydrophobic drugs (*i.e.*, paclitaxel and withaferin A) through a co-incubation method^{12,26}. However, due to their high hydrophilicity, biomacromolecular drugs such as peptide/protein drugs were not appropriate for this method.

Therefore, a sonication method was developed for the preparation of insulin-loaded exosomes (EXO@INS). As shown in Fig. 2A, the DLS size of EXO@INS was 71.9 nm, which was similar to that of drug-free EXOs. A slight decrease in the zeta potential from -9.8 to -12.4 mV was observed following INS encapsulation. TEM images showed that the typical morphology was maintained after sonication (Fig. 2B). The drug loading efficiency and encapsulation efficiency of INS was 57.7% (*w/w*) and 15.9% respectively, which was sufficiently high for oral administration.

Subsequently, gel electrophoresis and Coomassie staining experiments showed similar protein compositions between EXO@INS and EXO (Fig. 2C). This result demonstrates that exosomal proteins that contribute to “exosome–cell communication” were preserved after the sonication process²⁶. Further, trypan blue quenching experiment was used to confirm the location of loaded INS. As shown in Fig. 2D, more than 60% of fluorescence intensity remained after trypan blue quenching process, indicating that most of FITC-INS was encapsulated in the interior of EXOs. The hypoglycemic activity of INS loaded in EXO was tested. As shown in Fig. 2E, INS released from EXO@INS (2 IU/Kg) and free INS (2 IU/kg) induced similar profiles of blood glucose change in mice after subcutaneous injection, which strongly demonstrated the bioactivity was preserved after the loading procedure.

EXO@INS exhibited no significant size increase in SGF, SIF and PBS (pH = 7.4) during incubation for 8 h (Fig. S3D). Subsequently, the release of INS in SGF (2 h) and SIF (6 h) was investigated. As shown in Fig. 2F, 68.9% of INS was released after 8 h, and no burst release in SGF was observed. As reported, some liposomes and polymer vesicles exhibited burst release of macromolecular drugs in acidic environments or PBS^{15,27}. Therefore, EXOs had relatively sustained release of INS and provide improved solutions to drug leakage problems. Furthermore, we explored whether EXOs could protect INS from enzymatic degradation. As shown in Fig. 2G and H, when incubated with trypsin and pepsin, free INS was almost completely degraded within 2 h. In contrast, only 20% of INS was degraded after 8 h incubation with trypsin and nearly 80% of INS remained intact after 2 h (time for EXO@INS to pass through the stomach) incubation with pepsin, which demonstrated that encapsulation enhanced the enzymatic stability of INS.

Our study provides the first demonstration of the encapsulation of protein/peptide into EXOs. Electrophoresis was the most widely used method for passive loading of miRNAs into exosomes, but is poorly suitable for protein/peptide encapsulation. To this end, some reports proposed an active loading method through endogenous biogenesis processes. However, this method was relatively complex and not suitable for the encapsulation of INS into EXOs. Sonication has been used to incorporate enzyme into exosomes, but a suboptimum sonication process might lead to irregular transformation of exosomes²⁸, which could disturb exosome–cell communication. Here, our optimized mild preparation approach by sonication was simple and scalable, and did not influence exosomal characteristics or the bioactivity of INS. Moreover, EXO@INS had good colloidal stability and significantly enhanced the enzymatic stability of INS, indicating the feasibility of EXOs as an alternative oral nano-vehicle.

3.3. EXO@INS elicited a strong hypoglycemic effect and enhanced oral bioavailability of insulin

Glucose tolerance test (GTT) was performed to evaluate the oral delivery efficiency of EXO@INS. The doses of EXO@INS were 30

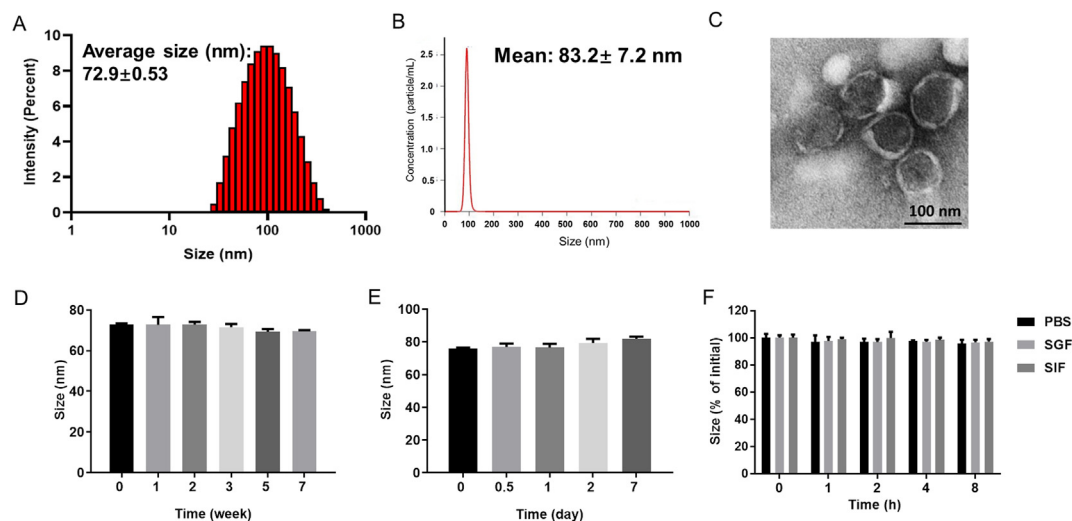


Figure 1 Characterization of exosomes (EXOs). (A) Size detected by dynamic light scattering (DLS). (B) Size detected by nanoparticle-tracking analysis (NTA). (C) TEM images of EXOs. Scale bar: 100 nm. Size of EXOs stored for -80°C (D) and 4°C (E). (F) The size variation of EXOs in stimulated gastric fluid (SGF), stimulated intestinal fluid (SIF) and PBS during 8 h. Error bars represent SD ($n = 3$).

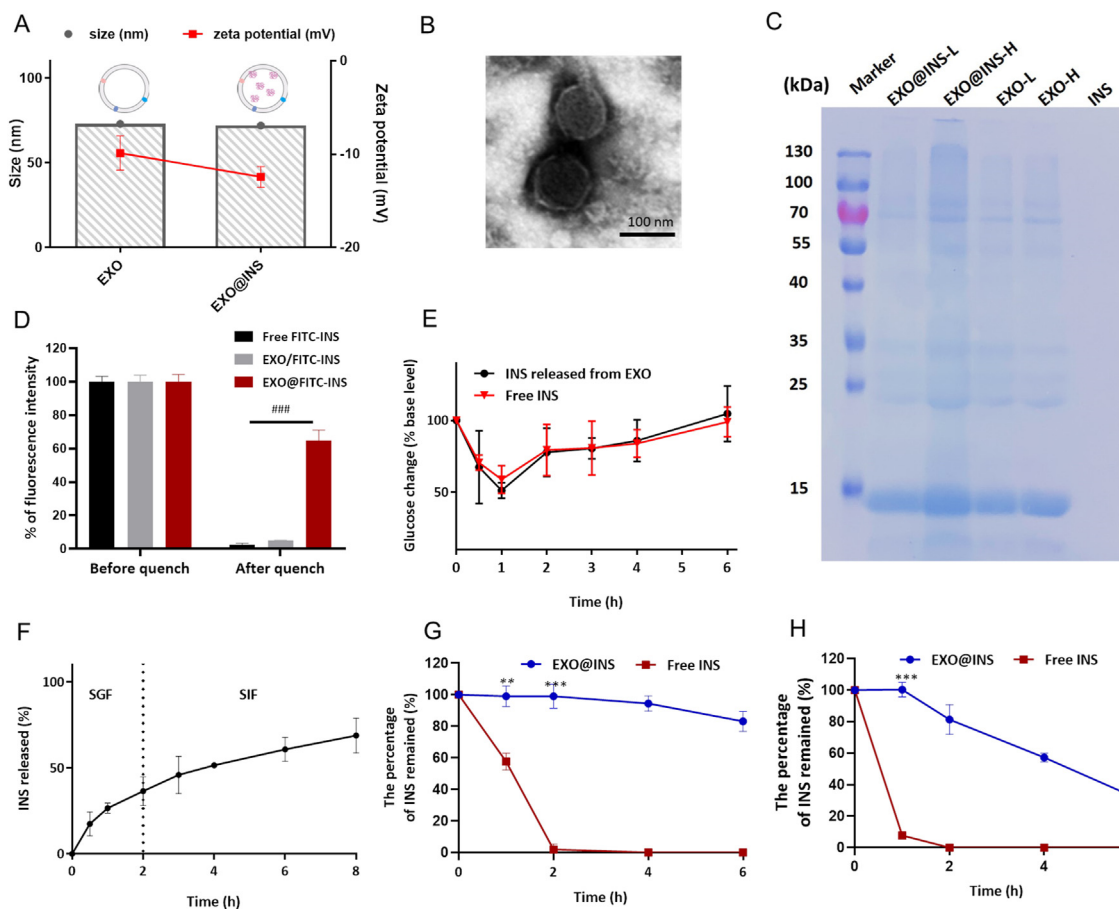


Figure 2 Characterization of EXO@INS. (A) DLS size and zeta potential of EXOs and EXO@INS. Error bars represent SD ($n = 3$). (B) TEM image of EXO@INS. Scale bar: 100 nm. (C) The protein bands after Coomassie staining. L: low concentration. H: high concentration. INS: free insulin solution. (D) Fluorescence intensity of FITC-INS before and after trypan blue quenching, $###P < 0.001$. Error bars represent SD ($n = 3$). (E) Changes in blood glucose after subcutaneous injection of free INS and released INS. Error bars represent SD ($n = 5$). (F) Release of insulin from EXO@INS in SGF and SIF. Error bars represent SD ($n = 3$). (G) The percentage of INS remained in trypsin solution (75 IU/mL). $**P < 0.01$, $***P < 0.001$, versus the Free INS group. Error bars represent SD ($n = 3$). (H) The percentage of INS remained in pepsin solution (12.5 IU/mL). $***P < 0.001$ versus the Free INS group. Error bars represent SD ($n = 3$).

and 50 IU/kg. As shown in Fig. 3A, the glucose level in the saline group exhibited a sharp increase and peaked (14.7 mmol/L) after 30 min after glucose administration. When EXO@INS (30 IU/kg) was orally administered 2 h prior to glucose challenge, an almost equal reduction effect in the blood glucose level (BGL) with subcutaneous injection (s.c.) group was observed. Moreover, EXO@INS (50 IU/kg) exhibited a more obvious reduction of BGL, with a peak of 8.0 mmol/L. Excitingly, the maximum BGL reduction obtained with EXO@INS (50 IU/kg) was even stronger than that observed in the s.c. group, which indicated the superiority of EXOs as oral vehicles. The area under the curve (AUC) of the blood glucose was calculated (Fig. 3B). The AUC obtained with EXO@INS (50 IU/kg) was markedly lower than that obtained with the saline group ($P < 0.001$) and was even lower than that observed with the s.c. group ($P < 0.05$). Therefore, EXO@INS could significantly improve the glucose tolerance of mice.

The hypoglycemic effect and pharmacokinetic behaviors on type I diabetic rats were then studied. The doses of EXO@INS were set to 18, 30 and 50 IU/kg. Fig. 3C showed that, compared with that observed with normal saline group, the oral administration of INS solution (50 IU/kg) or INS-free EXOs did not decrease BGL, whereas EXO@INS (18 IU/kg) exerted a significant hypoglycemic effect. Moreover, the hypoglycemic response of EXO@INS was dose-dependent. Impressively, EXO@INS (50 and 30 IU/kg) elicited a more superior and more sustained hypoglycemic effect with a maximal BGL reduction to 30% and 35%, compared with that obtained with subcutaneously injected

INS. The relative bioavailability of EXO@INS (30 IU/kg) was 10.6-fold higher than that of free INS (Table 1).

It should be noted that the therapeutic effect of EXO@INS was stronger than that of some of our previously developed nanoplateforms, such as solid lipid nanoparticles (SLNs) and PEGylated polymeric nanoparticles (NPs)^{29,30}. Besides, although there were a large number of studies on oral delivery of insulin using lipid-based nanocarriers, EXOs provided an organic solvent-free preparation procedure and avoided complex ligand modification. Therefore, the enhanced *in vivo* hypoglycemic efficacy and oral bioavailability of INS indicated the feasibility of EXOs as efficient vehicles for peptide/protein drugs. Additionally, the yield of EXOs was higher than that of exosomes from patients' body fluids or cell culture media, which made their large-scale production feasible.

3.4. Milk-derived exosomes exhibited efficient internalization by active multi-targeting to the epithelia

For transportation into the bloodstream, nanoparticles first need to overcome cellular permeability barrier. According to previous reports, we prepared a commonly used oral vehicle PEG coated poly (lactic-co-glycolic acid) (PLGA)-based nanoparticles (PPNs)³¹. Impressively, the cellular internalization of EXOs in E12 cells and Caco-2 cells was 8.9-fold and 8.6-fold higher than that of PPNs ($P < 0.01$, Fig. 4A). Representative fluorescence images also reflected the higher internalization of EXOs, which indicated stronger

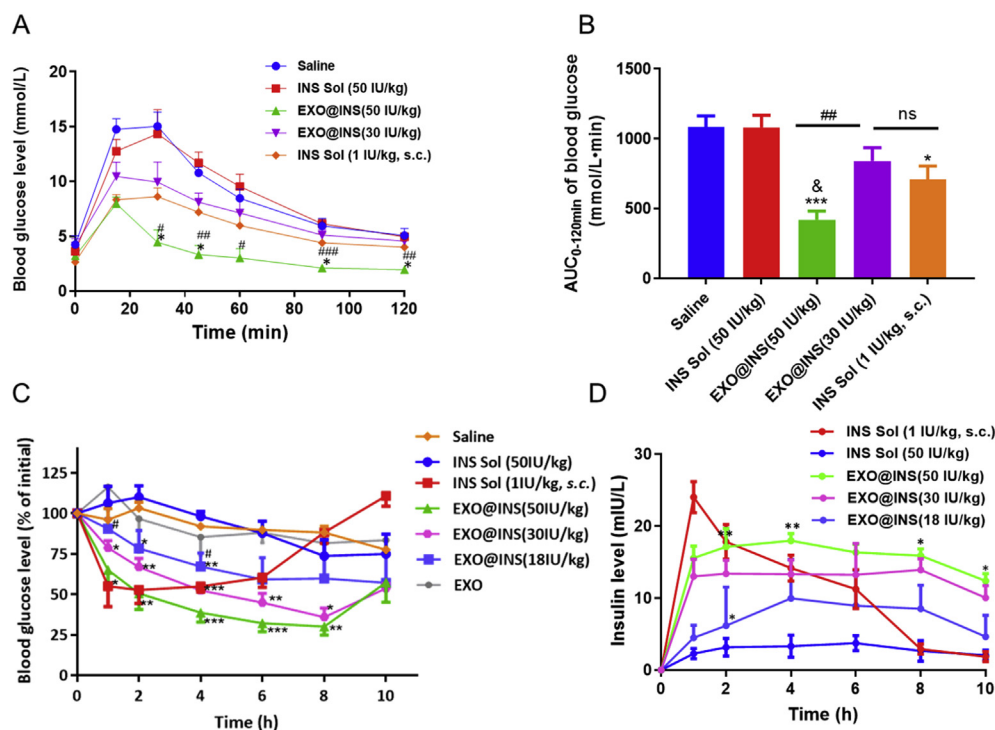


Figure 3 *In vivo* therapeutic effect of EXO@INS. (A) Blood glucose level in the glucose tolerance test (GGT) assay. * $P < 0.05$ versus INS Solution (INS Sol, 1 IU/kg, s.c.). # $P < 0.05$, ## $P < 0.01$, ### $P < 0.001$, versus EXO@INS (30 IU/kg). Error bars represent SD ($n = 5$). (B) AUC of blood glucose in the GGT assay. * $P < 0.05$, *** $P < 0.001$ versus Saline. &<0.05 versus INS Solution (INS Sol, 1 IU/kg, s.c.), ## $P < 0.01$, ns, not significant. Error bars represent SD ($n = 5$). (C) The blood glucose variation in type I diabetic rats. * $P < 0.05$, ** $P < 0.01$, *** $P < 0.001$, versus INS Solution (INS Sol, 50 IU/kg). # $P < 0.05$, ## $P < 0.01$, versus EXO@INS (50 IU/kg). Error bars represent SEM ($n = 5$). (D) Plasma insulin level after administration of insulin solution (INS Sol, 1 IU/kg, s.c.), insulin solution (INS Sol, 50 IU/kg, p.o.), EXO@INS (p.o.). * $P < 0.05$, ** $P < 0.01$, versus EXO@INS (30 IU/kg). Error bars represent SEM ($n = 5$).

Table 1 Pharmacokinetic parameters of plasma insulin in diabetic rats.

| Sample | Dose (IU/kg) | AUC _{0-10h} ($\mu\text{IU}\cdot\text{h/mL}$) | Fr (%) | PA (%) |
|---------------------|--------------|---|--------|--------|
| INS solution (s.c.) | 1 | 109.2 \pm 14.8 | — | — |
| INS solution (p.o.) | 50 | 21.0 \pm 12.7 | 0.38 | 0.025 |
| EXO@INS | 50 | 205.3 \pm 15.9*** | 3.76 | 4.33 |
| EXO@INS | 30 | 132.1 \pm 20.0 | 4.03 | 5.69 |
| EXO@INS | 18 | 73.2 \pm 32.6* | 3.72 | 5.92 |

Each value represents the mean \pm SD ($n = 5$). AUC: area under the plasma concentration–time curve; Fr (%): relative bioavailability; PA (%): pharmacological availability. * $P < 0.05$, *** $P < 0.001$, versus EXO@INS (30 IU/kg). —Not applicable.

membrane affinity (Fig. 4B). Having demonstrated the desirable cell internalization of EXOs, we explored the endocytic mechanisms. First, co-incubation with NaN_3 , a disruptor of adenosine triphosphate, decreased the uptake of EXOs to 78% ($P < 0.05$, Fig. 4C), indicating the involvement of energy-dependent endocytosis. Moreover, TEM images of EXO-treated Caco-2 cells reflected the interaction between EXOs and cell membrane. The internalization of EXOs, membrane invagination and membrane deformation were observed (arrow pointed, Fig. 4D), which indicated the endocytosis of EXOs. Different endocytic pathways were then

blocked by specific inhibitors. As shown in Fig. 4C, inhibitors of the caveolae-mediated pathway (lovastatin and filipin), clathrin-mediated pathway (chlorpromazine) and micropinocytosis (wortmannin and amiloride) all significantly decreased the uptake of EXOs, suggesting multiple endocytic pathways. Moreover, the uptake was not suppressed by M- β -CD, an inhibitor of lipid raft-dependent endocytosis. Although some researchers proposed the direct fusion of exosomes with the cell membrane³², the suppression of uptake by specific inhibitors demonstrated that EXOs were at least partially internalized *via* multiple endocytic routes.

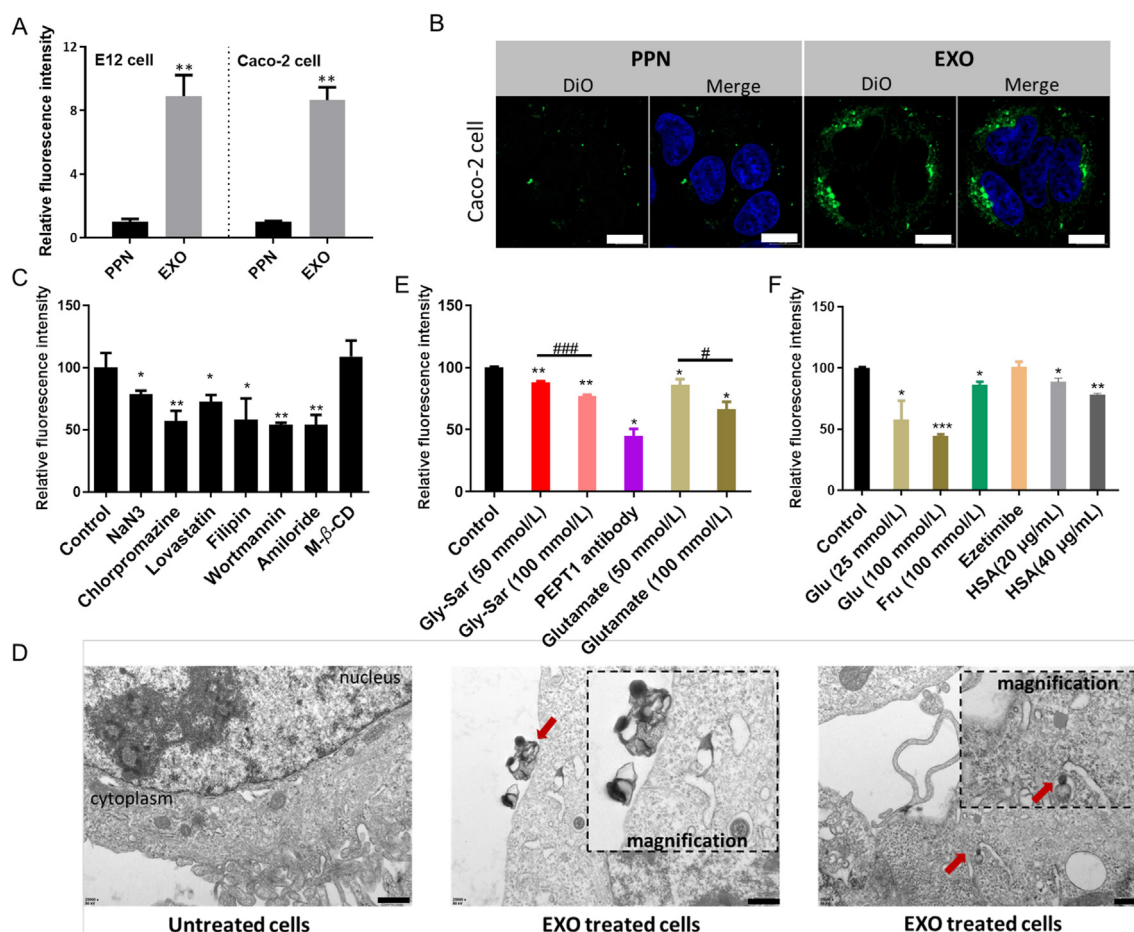


Figure 4 The mechanisms of cellular uptake. (A) Cellular uptake of PPNs and EXOs in E12 cells (with post-removal of mucus) and Caco-2 cells. ** $P < 0.01$ versus PPN. (B) CLSM images of DiO-loaded PPNs or EXOs treated Caco-2 cells. Blue: nucleus. Scale bar: 10 μm . (C, E, F) Cellular uptake of EXO@DiI with the addition of different inhibitors. Glu: glucose; Fru: fructose. HSA: human serum albumin. * $P < 0.05$, ** $P < 0.01$, *** $P < 0.001$, versus control. # $P < 0.05$, ### $P < 0.001$. Error bars represent SD ($n = 3$). (D) TEM images of Caco-2 cells with or without EXOs treatment. EXOs that interacted with cell membrane and internalized EXOs were indicated by red arrows. Scale bar: 500 nm.

Because EXOs were derived from nutrients, we speculated that they were ingested *via* the nutrient-assimilation pathway. First, glycylsarcosine (Gly-Sar), an inhibitor of peptide transporter (PEPT1), significantly decreased the uptake of EXOs in a dose-dependent manner (Fig. 4E). The inhibitory effect of the PEPT1 antibody (45%, $P < 0.05$) further demonstrated the involvement of PEPT1 during endocytosis. Furthermore, glutamate competitively inhibited the uptake of EXOs in a dose-dependent manner, which suggested the mediation of acid amino transporters. Glucose and fructose both decreased the uptake of EXOs (Fig. 4F), indicating the mediation of glucose transporters. Moreover, the decrease of fluorescence within cells caused by human serum albumin (HSA) indicated that the neonatal Fc receptor (FcRn) was involved in endocytosis (Fig. 4F). However, the uptake of EXOs was not affected by ezetimibe, which is an inhibitor of Niemann-Pick C1-like 1 (NPC1L1) and mediates the absorption of cholesterol and phytosterols (Supporting Information Fig. S4). Therefore, we speculated that unique surface characteristics enabled the efficient internalization of EXOs by active multi-targeting to the epithelia.

Due to the complex exosomal compositions, more receptors and transporters need to be investigated to comprehensively elucidate endocytic mechanisms. According to a previous report, targeting efficiency of ligand-modified NPs could be affected by receptor saturation and distribution density³³. Herein, compared with artificially synthesized NPs, the endocytosis of EXOs involved multiple targets. It was thus speculated that the nature of the receptor had less influence on EXOs active uptake. For the future construction of oral delivery vehicles, multi-ligand modification strategy can be considered to mimic EXOs. Of course, the types and ratio of the ligands need to be further screened.

3.5. Milk-derived exosomes could adapt to variable environmental pH during trafficking

The complex pH variation along the oral route constitutes another obstacle to drug delivery. Drug-loaded vehicles pass through the highly acidic stomach, the nearly neutral enteric cavity, the acidic intracellular vesicles (*i.e.*, early endosome, late endosome and lysosome) and finally enter the circulating system (pH 7.4). Interestingly, EXOs and their encapsulated cargo reportedly survive the harsh gastric conditions during transportation³⁴, which might indicate the intrinsic ability of EXOs to adapt to pH variation. Whether EXOs adapt to the above-mentioned pH changes and the relationship between variable pH and EXOs transport remain unanswered questions, and further studies were performed.

3.5.1. Milk-derived exosomes tailored the membrane rigidity to withstand highly acidic environment

EXOs were highly resistant to harsh environments in the GIT³⁵, the underlying mechanisms were unclear. Considering mechanical rigidity is one of the determinants of lipid vehicle's stability, we evaluated the membrane rigidity of EXOs under different pH conditions. Laurdan (2-dimethylamino-6-laruroylnaphthalene) intercalates into lipid bilayers and exhibits different emission properties based on the degree of order. Tightly ordered lipids shift the maximum emission spectrum to 435 nm, whereas peak at 490 nm in a disordered state. The generalized polarization (GP) index [$GP = (I_{435} - I_{490}) / (I_{435} + I_{490})$] can be calculated to

distinguish the order degree of the lipid membrane³⁶. As shown in Fig. 5A, EXOs in acidic environments exhibited higher GP values ($P < 0.01$), which indicated a significantly more compact structure for the maintenance of stability. Young's modulus investigation showed similar results (Fig. 5B). Moreover, the structural transition was reversible when the pH shifted from 2 to 7.4 ($P < 0.01$). In other words, EXOs exhibited good membrane fluidity and interacted with the cell membrane when they reached the intestinal tract (Fig. 4D).

3.5.2. Milk-derived exosomes avoided endo-lysosomal trapping in a pH-dependent manner

After endocytosis, EXOs are packed into acidic intracellular vesicles. Endosomes and lysosomes are considered a main trafficking barrier to protein drugs³⁷. An acidic environment with abundant enzymes results in degradation of NPs and trapped macromolecules²⁹. As shown in Fig. 5A, EXOs exhibited high membrane rigidity within the acidic environment in endo-lysosome (pH 5.5). Interestingly, according to previous report, NPs with compact structure were more likely to escape endosomal confinement³⁸. Thus, whether EXOs have an inherent ability to avoid endo-lysosomal trapping remains unclear. First, specific inhibitors of the lysosomal pathway were utilized. Chloroquine and LY294002 did not affect trafficking and exocytosis (Supporting Information Fig. S5). Additionally, EXOs and lysosomes showed no obvious colocalization, and the Pearson's correlation coefficient (Rr) was 0.44 (Fig. 5C). To further investigate whether EXOs avoided endo-lysosomal trapping, we labeled the endosomes by immunostaining with specific antibodies (Fig. 5D). Results showed that EXOs did not exhibit obvious co-localization in early-, late- and recycling endosomes. The Rr values of these organelles were all less than 0.5 (Fig. 5E). To explore the relationship between pH and the avoidance of endo-lysosomal confinement, we performed a hemolysis assay with red blood cells (RBCs) under different pH conditions. PPNs that went through endo-lysosomal pathway were investigated as a negative control (Supporting Information Fig. S6). The hemagglutinin-2 (GLFEAIEGFIENGWEGMIDGWYG, HA2) peptide, an endosome disruptor, was used as a positive control²⁹. At pH 7.4, all these groups showed low hemolysis efficiency (<10%), which indicated the intactness of the cell membrane in physiological conditions. Notably, early endosomes and lysosomes-mimetic pH environments (pH 6.5 and 5.5) sharply increased the hemolysis efficiency of EXOs to 73% and 90%, respectively (Fig. 6A). HA2 elicited a similar hemolytic effect as the pH decreased, whereas PPNs still showed low hemolysis efficiency. The pH-sensitive hemolytic activity indicated that EXOs could fuse with the membrane of endo/lysosomes, and this fusing enabled endo-lysosomal escape. EXO@FITC-INS/Dil was found to transport across Caco-2 cell monolayer with intact form (Supporting Information Fig. S7), and EXO@INS were able to transverse Caco-2 cell monolayer and intestine without the change of morphology (Fig. 6B), indicating that avoidance of endo-lysosomal confinement significantly improved the stability of EXOs and loaded drugs.

3.5.3. Milk-derived exosomes traversed the intestinal epithelium to the bloodstream adapting to pH variations

It was reported that acidic tumor microenvironment played an important role in exosomes internalization³⁹. Coincidentally, intestinal cavity presents a weakly acidic environment. Therefore,

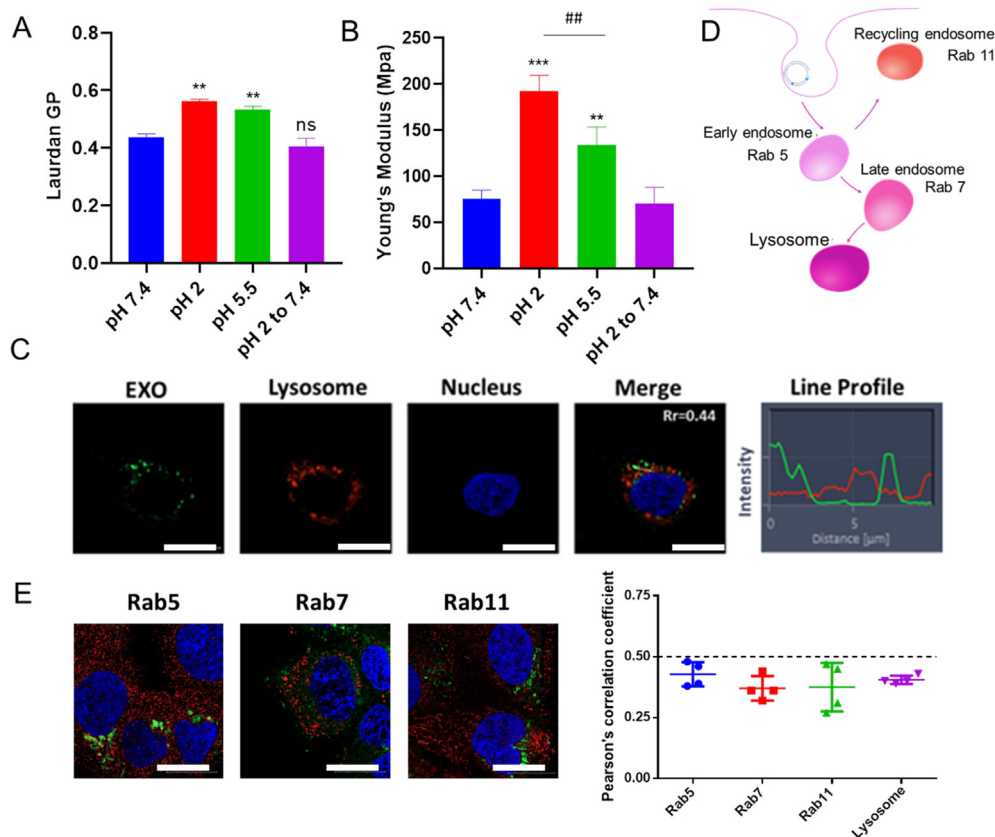


Figure 5 Membrane rigidity and intracellular trafficking pathway of EXO. (A) Laurdan GP values (excitation wavelength of 340 nm). $***P < 0.01$ versus pH 7.4. ns, not significant. Error bars represent SD ($n = 3$). (B) Young's modulus of EXOs under different pH. $***P < 0.001$ and $**P < 0.01$ versus pH 7.4. $##P < 0.01$. Error bars represent SD ($n = 3$). (C) CLSM images of EXOs treated cells. The Rr and line profile were measured. Scale bar: 20 μm (D) Scheme of the endo-lysosomal pathway and specific protein markers. (E) Immunostaining images of Rab5, Rab7 and Rab11 (red). Green fluorescence represents EXO@DiO. Scale bar: 20 μm . The Rr between organelles with EXO@DiO was determined. Error bars represent SD ($n = 3$).

whether the acidic pH in the intestinal tract also favored EXOs traffic in epithelium was unclear. Consistent with our hypothesis, a weakly acidic environment (pH 6.0) increased the uptake of EXOs (Fig. 6C). Moreover, at pH 7.4, lower fluorescence within cells was found following the exocytosis process (Fig. 6D). In other words, EXOs leveraged the pH gradient existing between the intestinal lumen and the bloodstream to facilitate transcytosis. According to previous findings, FcRn was one of the target sites of EXOs, which transported endogenous IgG in a pH-dependent manner⁴⁰. FcRn involved endocytosis might endow EXOs with the ability to adapt to pH changes. We then blocked the FcRn pathway with a high concentration of HSA (80 $\mu\text{g}/\text{mL}$). Interestingly, FcRn occupation only partly weakened the pH compliance of EXOs (Fig. 6E and F), indicating that other mechanisms were involved in the pH-adaptive transcytosis of EXOs besides FcRn targeting. It might ascribed to the unique membrane composition of EXOs.

Taken together, this study provides the first demonstration that EXOs can take advantage of the variable pH during trafficking to maintain their stability under extremely acidic conditions, avoid endo-lysosomal confinement and promote uptake and exocytosis. Their pH adaptation attributed to timely adjustment of the membrane rigidity and was partly due to FcRn-targeting. The mechanisms underlying the observed pH-dependent membrane variations were likely due to the unique lipid compositions of EXOs⁴¹, which need to be studied further. To overcome the

variable environments during oral route, pH-responsive strategies and ligand optimization could be combined. Furthermore, the unique lipid composition of EXOs could be migrated to the construction of lipid-based nanoplat-forms in the future.

3.6. Milk-derived exosomes showed efficient apical-to-basolateral transport by targeting the ERK1/2 and p38 MAPK signaling pathways

Based on the polarized feature of intestinal epithelia, nanoplat-forms exhibit distinct exocytic behaviors from apical or basolateral side^{42,43}. Unfortunately, a large proportion of apical exocytosis severely hinders the ultimate delivery of a payload into the bloodstream even if the nanoplat-forms are efficiently internalized. Hence, we evaluated the exocytic mechanisms of EXOs. First, apparent permeability coefficient (Papp) value of EXOs was 4.5-fold enhanced compared with PPNs ($P < 0.01$, Fig. 7A). Then the bidirectional exocytosis rate was investigated using Transwell permeable supports (Fig. 7B). The exocytosis rate of PPNs from the basolateral side was only 78% of that from the apical side ($P < 0.001$, Fig. 7C), which was consistent with our previous study⁴². Impressively, EXOs showed a markedly higher proportion of basolateral exocytosis, which was 1.8-fold higher than that of apical exocytosis ($P < 0.001$). Furthermore, the transport rate from the apical to basolateral side was 2.8-fold higher than that in

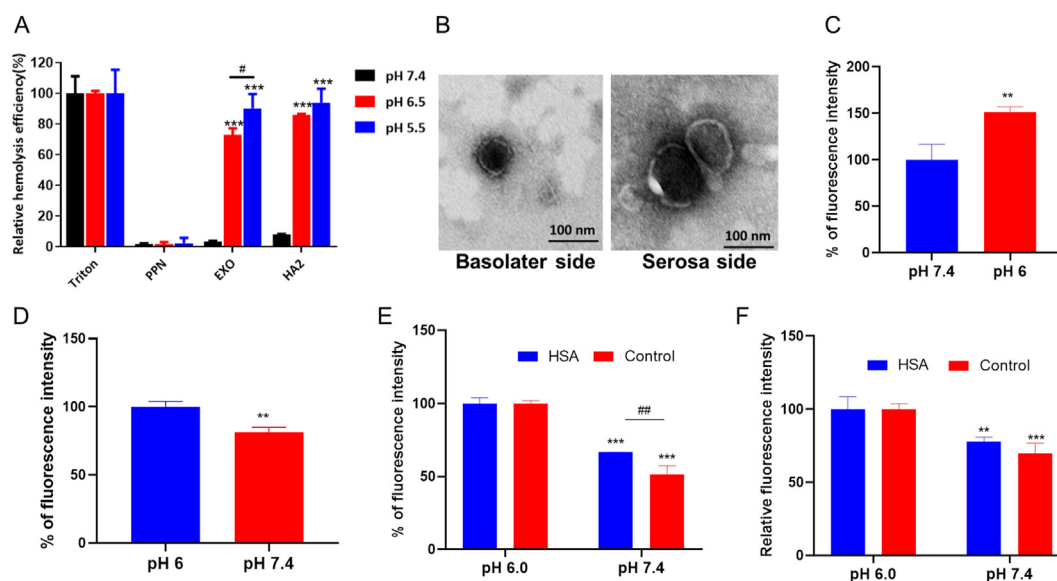


Figure 6 pH-Dependent hemolysis, uptake and exocytosis. (A) Hemolysis assay. The relative hemolysis efficiency of RBCs after incubation with PPNs, EXOs and HA2 under different pH conditions is shown. $***P < 0.001$ versus pH 7.4. $\#P < 0.05$. Error bars represent SD ($n = 3$). (B) TEM images of EXO@INS collected from the basolateral side of Caco-2 cell monolayer and serous side of detached intestine. Scale bar: 100 nm. (C) Cellular uptake of EXO@DiI under different pH. $**P < 0.01$ versus pH 7.4. Error bars represent SD ($n = 3$). (D) Fluorescence intensity of EXOs detained within cells. $**P < 0.01$, versus pH 6.0. Error bars represent SD ($n = 3$). (E) Cellular uptake of EXO@DiI under different pH conditions in the presence of excess HSA. $***P < 0.001$, versus pH 6.0, $###P < 0.01$. Error bars represent SD ($n = 3$). (F) The fluorescence intensity of EXOs detained within cells in the presence of excess HSA. $**P < 0.01$, $***P < 0.001$, versus pH 6.0.

the opposite direction ($P < 0.05$, Fig. 7D). The transepithelial electrical resistance (TEER) value of cell monolayer showed no significant change after EXOs-treatment (Supporting Information Fig. S8). Therefore, EXOs did not disrupt the integrity of the cell monolayer, excluding the paracellular route.

Recently, it's reported that cells may respond to incoming nanovesicles, which in turn promoted transcytosis⁴⁴. Therefore, whether EXOs had an intrinsic ability to trigger positive feedback and thus promote oral drug transportation is an interesting issue to be studied. Thus, we investigated the mechanisms in terms of signaling pathways related to EXOs trafficking. Mitogen-activated protein kinases (MAPKs) include ERK1/2 and p38 coordinate responses and serve as key sensors of the energy status within a cell¹⁶. MAPK activation is reportedly beneficial for nutrient absorption⁴⁵. Therefore, we hypothesized that EXOs transport might be facilitated by the MAPK pathway. First, we investigated the effect of MAPK agonist on the exocytosis efficiency of EXOs²³. As shown in Fig. 7E, insulin could promote EXO@DiI exocytosis in a concentration-dependent manner ($P < 0.001$). Although insulin was selected as the model drug in above study, the insulin encapsulated in EXOs wouldn't trigger signal activation. Western blotting further confirmed our hypothesis. ERK1/2 and p38 phosphorylation were stimulated after exposure to EXOs (Fig. 7F). As previously reported, activation of the p38 MAPK pathway contributed to the translocation of GLUT-2 to the apical membrane of intestinal epithelium²⁴. Interestingly, our finding showed that glucose transporter participated in the endocytic routes of EXOs (Fig. 4D), and GLUT-2 were able to facilitate the apical-to-basolateral migration of nanoformulations. Moreover, the fact that upregulating the MAPK pathway increased lipid absorption might be beneficial to lipid extracellular vesicle transcytosis⁴⁵. Blockage of the signaling pathway by the specific inhibitors U0126 and SB202190 sharply decreased exocytosis of

EXOs (Fig. 7G and H). According to a previous study, MAPK signaling was associated with endoplasmic reticulum/Golgi apparatus (ER/GA) secretory pathway. As shown in Fig. 7I, the cellular retention of EXOs was increased by co-incubation with monensin and brefeldin A, indicating endoplasmic reticulum (ER) and Golgi apparatus (GA)-related exocytosis pathway. Consistently, EXOs were colocalized with ER and GA, which was beneficial for basolateral exocytosis (Fig. 7J). In summary, the intestinal epithelium forms a key obstacle to quantities of cargo, but EXOs have a "pass permit". By talking to cells, EXOs triggered changes in cell signaling pathways to facilitate efficient apical-to-basolateral transport.

Our study demonstrated that EXOs overcame the obstacle of limited basolateral exocytosis by ensuring efficient apical-to-basolateral transport across the intestinal epithelia. However, increasing the basolateral exocytosis of many orally delivered NPs (e.g., gold NPs, SLNs and PEGylated polymeric NPs) is challenging^{42,43,46}. These results strongly demonstrate that "talking to cells" namely exploiting cell signal regulation is expected to be a valid strategy. Although MAPK is an alternative target, more signaling pathways involving polarized trafficking within the intestinal epithelium need to be investigated and exploited as novel targets.

3.7. Milk-derived exosomes are efficiently transported across the intestinal mucosa

The net-like mucus layer acts as a formidable barrier to most orally delivered NPs, which limits their access to underlying epithelial cells⁴⁷. Lenzini et al.⁴⁸ recently investigated the transport of extracellular vesicles (EVs) within the extracellular matrix (ECM). Matrix (ECM) stress relaxation and aquaporin-1-mediated EV deformability jointly promoted the EV transport in the ECM. However, whether EXOs can move freely in mucosa due to the

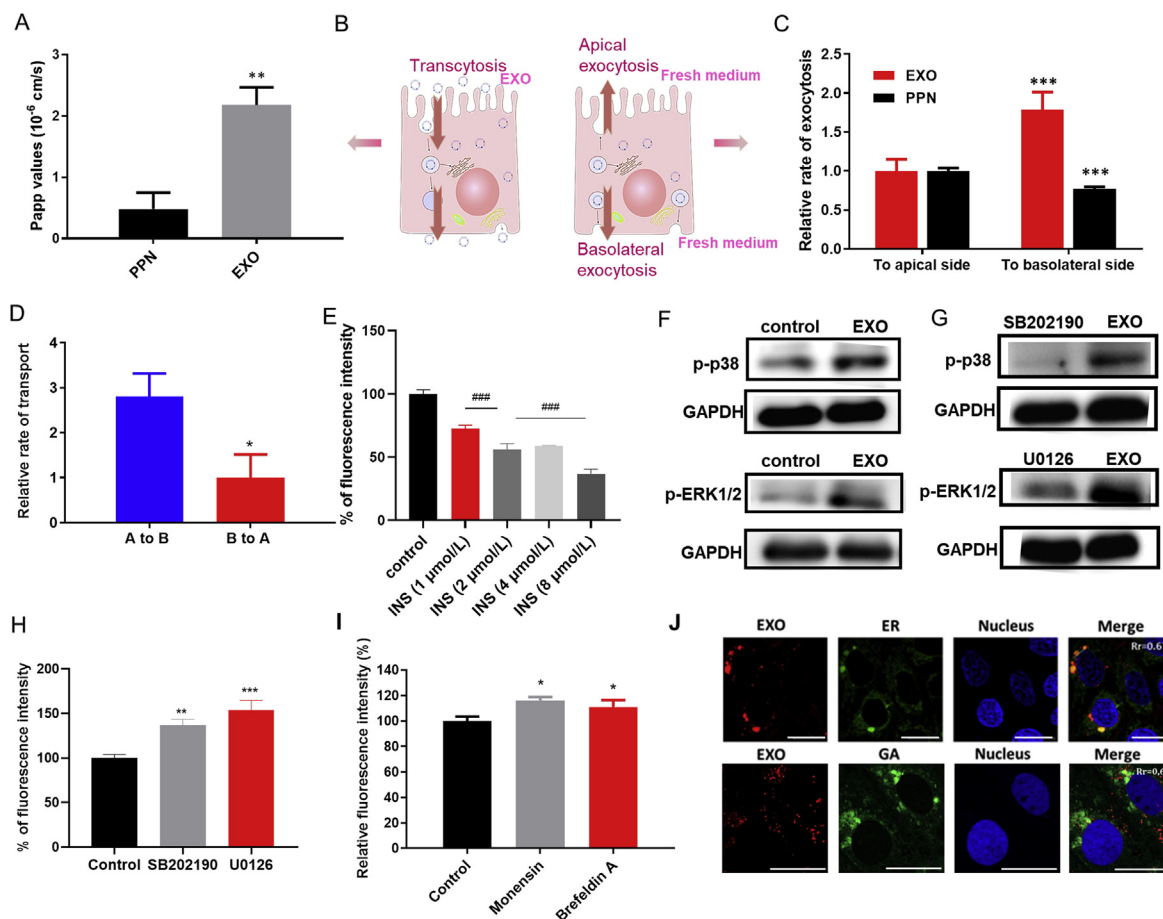


Figure 7 The mechanisms of transportation of EXO. (A) The Papp value of transportation across Caco-2 cell monolayer. $**P < 0.01$, versus PPN. Error bars represent SD ($n = 3$). (B) Scheme of the transcytosis and bidirectional exocytosis assay. (C) Relative exocytosis rate from apical and basolateral side. $***P < 0.001$, versus apical exocytosis. Error bars represent SD ($n = 3$). (D) Relative transport rate of EXOs in different orientations. A: apical side; B: basolateral side. $*P < 0.05$, versus A to B. Error bars represent SD ($n = 3$). (E) Exocytosis efficiency regulated by insulin in a dose-dependent manner. $###P < 0.001$. Error bars represent SD ($n = 3$). (F) Representative blot for p-ERK1/2, p-p38 and GAPDH in Caco-2 cells stimulated with EXOs for 30 min. (G) Representative blot for p-ERK1/2, p-p38 and GAPDH in Caco-2 cells in the presence of signaling pathway inhibitors. (H) Fluorescence intensity of EXOs detained within cells. $**P < 0.01$, $***P < 0.001$, versus control. Error bars represent SD ($n = 3$). (I) Fluorescence intensity of EXOs within cells. $*P < 0.05$, versus control. Error bars represent SD ($n = 3$). (J) CLSM images of EXOs treated cells. The Rr and line profile were measured. ER: endoplasmic reticulum; GA: Golgi apparatus. Scale bar: 20 μ m.

mesh-like structure of mucus and ECM is unclear. We evaluated the transport of EXOs across the intestinal mucosa whereas PPNs and mucoadhesive nanoparticles (MAPs) were treated as positive and negative controls. Also, distribution of free DiI was shown to prove that red fluorescence represented EXOs rather than dissociated DiI molecules. First, EXO@DiI displayed a uniform distribution within mucus following their oral administration to mice, and this distribution was similar to that observed with PPNs, in contrast, MAPs showed an aggregated and uneven distribution. Free DiI molecules aggregated heavily due to the hydrophobic interaction with mucus while EXO@DiI exhibited uniform distribution. This result confirmed that the red fluorescence represented distribution of EXOs rather than dissociated DiI (Fig. 8A and B). An *in vitro* three-dimensional Transwell model with porcine intestinal mucus showed that 3.5% of particles penetrated the basal chamber with both EXOs and PPNs, and this value was 3-fold higher than that obtained with MAPs ($P < 0.05$, Fig. 8C). Fig. 8D reflects that MAPs (green) were mainly located in the mucus layer (red), whereas PPNs and EXOs were both internalized into cells. The quantitative results showed that 34% of MAPs

associated with E12 cells were trapped in the mucus layer instead of being internalized into cells (Fig. 8E). In contrast, no obvious trapping of EXOs and PPNs was observed ($P > 0.05$). All the above-mentioned results indicate the EXOs were capable of avoiding mucus trapping similar to PPNs.

According to a previous report, surface properties (*i.e.*, hydrophilicity, charge neutrality and deformability) largely contributed to the mucus-penetrating ability. Because the main components of the exosomal membrane were phospholipids and proteins⁴⁹, EXOs likely have surface properties distinct from those of lipid- or PLGA-based NPs. Proteins might increase the hydrophilicity of EXOs and thus avoid hydrophobic interactions with mucin. Negative phospholipids helped eliminate mucin capture. Additionally, deformation of EXOs might occur during mucus penetration and contribute to high permeability⁵⁰. Taken together, tailoring of surface properties in various aspects endowed EXOs with mucus-penetrating capability. In other words, the deformability and electrical and hydrophilic/hydrophobic properties need to be modulated to overcome the mucosal barrier⁵¹. Moreover, the unique lipid compositions and hydrophilic/

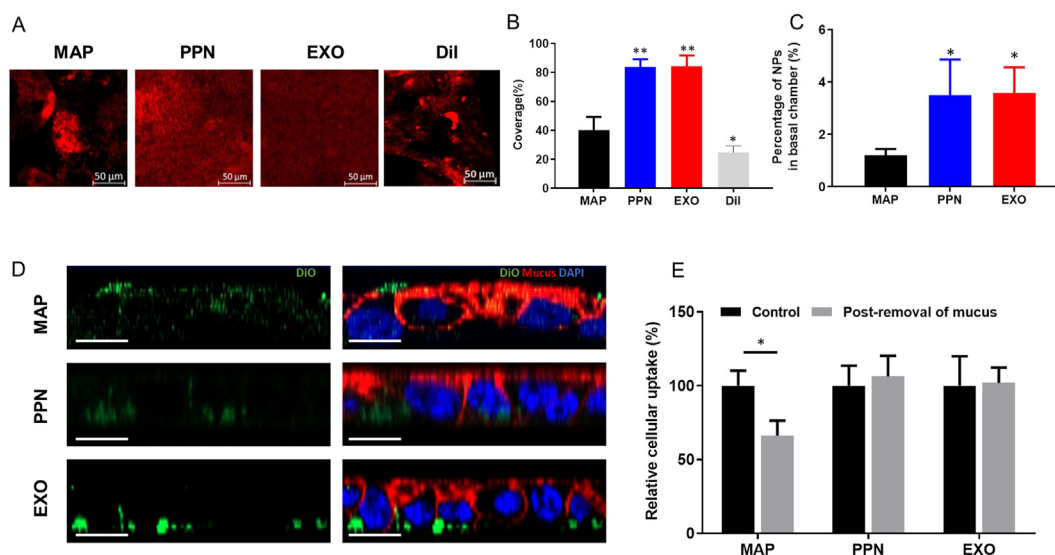


Figure 8 Study of mucus permeability. (A) Mucus distribution of DiI-loaded MAPs, PPNs, EXOs and free DiI in the intestine of mice after oral administration. (B) Calculated coverage (%) of particles in the intestinal mucus layer. * $P < 0.05$, ** $P < 0.01$, versus MAP. (C) Percentage of particles that permeated into the basal chamber across the mucus layer. * $P < 0.05$, versus MAP. (D) CLSM images of E12 cells after incubation with DiO-loaded MAPs, PPNs and EXOs (z -axis). Scale bar: 20 μm . (E) The cellular uptake with or without post-removal of mucus. * $P < 0.05$.

hydrophobic balance could be used as reference in the preparation of lipid-based nanocarriers to overcome mucus barriers.

3.8. Milk-derived exosomes were biocompatible oral nanoplatforms

In this section, safety evaluations of EXOs were performed both *in vitro* and *in vivo*. First, when the total exosomal protein was in the range of 25 to 250 $\mu\text{g/mL}$, EXOs showed no significant

influence on cell viability of typical cell models used to study oral administration (Fig. 9A), and the release of lactate dehydrogenase (LDH) was less than 10% (Fig. 9B). Therefore, EXOs were non-cytotoxic and showed no damage on membrane integrity. Subsequently, the hemolysis assay was performed with RBCs from rats. As shown in Fig. 9C, the hemolysis after EXOs treatment was less than 5%, indicating the good blood biocompatibility. Mice were then once-daily orally administered with EXOs for 7 consecutive days. The group administrated EXOs at varying doses (0.5, 1 and

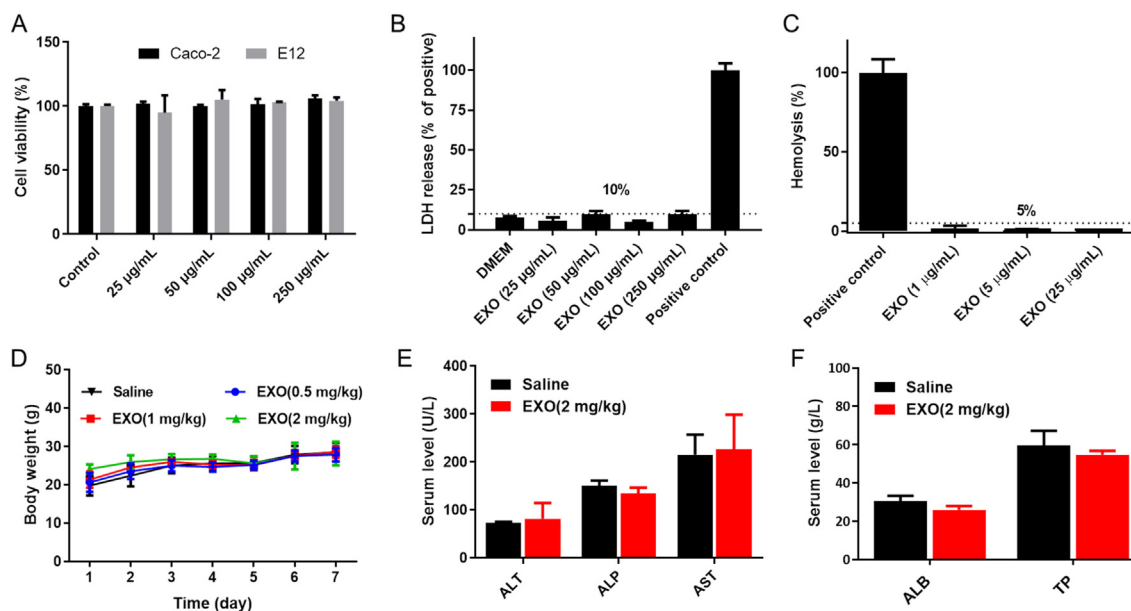


Figure 9 Study of biocompatibility. (A) Cell viability of Caco-2 and E12 cells after incubation with EXOs. Error bars represent SD ($n = 3$). (B) LDH release from Caco-2 cells after incubation with EXOs. Positive control: 1% Triton solution. Error bars represent SD ($n = 3$). (C) Hemolysis efficiency of RBCs after incubation with EXOs. Positive control: 1% Triton solution. Error bars represent SD ($n = 3$). (D) The body weight of ICR mice during the administration of EXOs or saline. Error bars represent SD ($n = 4$). (E, F) Levels of ALT, ALP, AST, ALB and TP after 7 consecutive days of oral administration of EXOs (2 mg/kg) or saline. Error bars represent SD ($n = 3$).

2 mg/kg) exhibited an increase in body weight similar to that observed in the saline group (Fig. 9D). After 7 days, the hematological parameters and serum chemistry of high-dosed group were analyzed. Supporting Information Table S1 shows that EXOs (2 mg/kg) did not induce adverse hematological effects. Moreover, the levels of alanine aminotransferase (ALT), alkaline phosphatase (ALP), aspartate aminotransferase (AST), albumin (ALB) and total protein (TP) showed no significant difference between the EXOs and saline group (Fig. 9E and F). Thus, oral administration of EXOs (2 mg/kg) did not damage the liver functions. Finally, a histopathology examination of the heart, liver, spleen, lung, kidney and small intestine was performed. All the EXOs-treated groups exhibited no obvious pathological changes, indicating good biocompatibility of EXOs to major organs and tissues (Supporting Information Fig. S9). Compared with inorganic nanomaterials⁵², EXOs are degradable and non-immunogenic as naturally equipped carriers. Because milk is a common nutrient source, EXOs are probably well tolerated for long-term administration. Consequently, preliminary evaluations demonstrated the biocompatibility of EXOs as oral drug delivery vehicles.

4. Conclusions

In this study, the novel insulin-loaded milk-derived exosomes (EXO@INS) was fabricated. EXO@INS elicited a more excellent and sustained hypoglycemic effect compared with that achieved with subcutaneously injected INS. Mechanism studies revealed that the excellent oral delivery ability of EXOs attributed to versatile effects include active multi-targeting uptake, pH adaptation during GI transit, nutrient assimilation related ERK1/2 and p38 MAPK signal pathway activation and intestinal mucus penetration. *In vitro* and *in vivo* safety evaluations demonstrated the biocompatibility of EXOs. Additionally, the simple and cost-effective approach for the preparation of EXO@INS contributed to their large-scale production. Taken together, the results demonstrated that EXOs exhibited great potential for the oral delivery of insulin, and offered new insights into developing naturally-equipped nanovehicles for oral administration.

Acknowledgments

We gratefully acknowledge financial support from the National Science Foundation for Distinguished Young Scholars (81625023, China), the National Natural Science Foundation of China (81872818), and the Major Research Plan of National Natural Science Foundation of China (81690261).

Author contributions

Lei Wu, Lingling Wang carried out the experiment, analyzed data and drafted the manuscript. Xi Liu, Yuli Bai, Ruinan Wu, Xiang Li and Yutong Mao participated part of the experiments. Ling Zhang, Yongxiang Zheng contributed to paper revision. Tao Gong and Zhirong Zhang are responsible for supervision. Yuan Huang came up with ideas, wrote and polished this manuscript. All of the authors have read and approved the final manuscript.

Conflicts of interest

The authors have no conflicts of interest to declare.

Appendix A. Supporting information

Supporting data to this article can be found online at <https://doi.org/10.1016/j.apsb.2021.12.015>.

References

- Moroz E, Matoori S, Leroux JC. Oral delivery of macromolecular drugs: where we are after almost 100 years of attempts. *Adv Drug Deliv Rev* 2016;**101**:108–21.
- Anselmo AC, Gokarn Y, Mitragotri S. Non-invasive delivery strategies for biologics. *Nat Rev Drug Discov* 2019;**1**:19–40.
- Yang BW, Chen Y, Shi JL. Exosome biochemistry and advanced nanotechnology for next-generation theranostic platforms. *Adv Mater* 2019;**2**:e1802896.
- Aqil F, Munagala R, Jeyabalan J, Agrawal AK, Kyakulaga AH, Wilcher SA, et al. Milk exosomes—natural nanoparticles for siRNA delivery. *Cancer Lett* 2019;**449**:186–95.
- Li D, Yao SR, Zhou ZF, Shi J, Huang ZH, Wu ZM. Hyaluronan decoration of milk exosomes directs tumor-specific delivery of doxorubicin. *Carbohydr Res* 2020;**493**:108032.
- Rufino-Ramos D, Albuquerque PR, Carmona V, Perfeito R, Nobre RJ, Pereira de Almeida L. Extracellular vesicles: novel promising delivery systems for therapy of brain diseases. *J Control Release* 2017;**262**:247–58.
- Somiya M, Yoshioka Y, Ochiya T. Biocompatibility of highly purified bovine milk-derived extracellular vesicles. *J Extracell Vesicles* 2018;**1**:1440132.
- Ahadian S, Finbloom JA, Mofidfar M, Diltemiz SE, Nasrollahi F, Davoodi E, et al. Micro and nanoscale technologies in oral drug delivery. *Adv Drug Deliv Rev* 2020;**157**:37–62.
- Bakhrui SH, Furtado S, Morello AP, Mathiowitz E. Oral delivery of proteins by biodegradable nanoparticles. *Adv Drug Deliv Rev* 2013;**6**:811–21.
- Benmoussa A, Lee CHC, Laffont B, Savard P, Laugier J, Boilard E, et al. Commercial dairy cow milk microRNAs resist digestion under simulated gastrointestinal tract conditions. *J Nutr* 2016;**11**:2206–15.
- Munagala R, Aqil F, Jeyabalan J, Gupta RC. Bovine milk-derived exosomes for drug delivery. *Cancer Lett* 2016;**1**:48–61.
- Agrawal AK, Aqil F, Jeyabalan J, Spencer WA, Beck J, Gachuki BW, et al. Milk-derived exosomes for oral delivery of paclitaxel. *Nano-medicine* 2017;**5**:1627–36.
- Liu X, Wu RN, Li YT, Wang LL, Zhou R, Li L, et al. Angiopep-2-functionalized nanoparticles enhance transport of protein drugs across intestinal epithelia by self-regulation of targeted receptors. *Biomater Sci* 2021;**8**:2903–16.
- Wolf T, Baier SR, Zempeni J. The intestinal transport of bovine milk exosomes is mediated by endocytosis in human colon carcinoma Caco-2 cells and rat small intestinal IEC-6 cells. *J Nutr* 2015;**10**:2201–6.
- Xiong XY, Li YP, Li ZL, Zhou CL, Tam KC, Liu ZY, et al. Vesicles from Pluronic/poly(lactic acid) block copolymers as new carriers for oral insulin delivery. *J Control Release* 2007;**1**:2:11–7.
- Yin LJ, Gupta R, Vaught L, Grosche A, Okunieff P, Vidyasagar S. An amino acid-based oral rehydration solution (AA-ORS) enhanced intestinal epithelial proliferation in mice exposed to radiation. *Sci Rep* 2016;**6**:37220.
- Yoshida K, Sato K, Anzai JI. Layer-by-layer polyelectrolyte films containing insulin for pH-triggered release. *J Mater Chem* 2010;**8**:1546–52.
- Fan WW, Xia DN, Zhu QL, Li XY, He SF, Zhu CL, et al. Functional nanoparticles exploit the bile acid pathway to overcome multiple barriers of the intestinal epithelium for oral insulin delivery. *Bio-materials* 2018;**151**:13–23.
- Wu L, Bai YL, Wang LL, Liu X, Zhou R, Li L, et al. Promoting apical-to-basolateral unidirectional transport of nanoformulations by manipulating the nutrient-absorption pathway. *J Control Release* 2020;**323**:151–60.

20. Shan W, Zhu X, Tao W, Cui Y, Liu M, Wu L, et al. Enhanced oral delivery of protein drugs using zwitterion-functionalized nanoparticles to overcome both the diffusion and absorption barriers. *ACS Appl Mater Interfaces* 2016;**38**:25444–53.
21. Zheng Z, Li ZF, Xu CC, Guo B, Guo PX. Folate-displaying exosome mediated cytosolic delivery of siRNA avoiding endosome trapping. *J Control Release* 2019;**311–312**:43–9.
22. Zhang SH, Ren M, Zeng XF, He PL, Ma X, Qiao SY. Leucine stimulates ASCT2 amino acid transporter expression in porcine jejunal epithelial cell line (IPEC-J2) through PI3K/Akt/mTOR and ERK signaling pathways. *Amino Acids* 2014;**12**:2633–42.
23. Gartz M, Darlington A, Afzal MZ, Strande JL. Exosomes exert cardioprotection in dystrophin-deficient cardiomyocytes via ERK1/2-p38/MAPK signaling. *Sci Rep* 2018;**1**:16519.
24. Pieri M, Christian HC, Wilkins RJ, Boyd CA, Meredith D. The apical (hPepT1) and basolateral peptide transport systems of Caco-2 cells are regulated by AMP-activated protein kinase. *Am J Physiol Gastrointest Liver Physiol* 2010;**1**:G136–43.
25. Carbolante G, Mantaj J, Ferrari E, Vllasaliu D. Cow milk and intestinal epithelial cell-derived extracellular vesicles as systems for enhancing oral drug delivery. *Pharmaceutics* 2020;**3**:266.
26. Manca S, Upadhyaya B, Mutai E, Desaulniers AT, Cederberg RA, White BR, et al. Milk exosomes are bioavailable and distinct micro-RNA cargos have unique tissue distribution patterns. *Sci Rep* 2018;**1**:11321.
27. Parmentier J, Becker MM, Heintz U, Fricker G. Stability of liposomes containing bio-enhancers and tetraether lipids in simulated gastrointestinal fluids. *Int J Pharm* 2011;**1**:2:210–7.
28. Haney MJ, Klyachko NL, Zhao Y, Gupta R, Plotnikova EG, He Z, et al. Exosomes as drug delivery vehicles for Parkinson's disease therapy. *J Control Release* 2015;**207**:18–30.
29. Xu YN, Zheng YX, Wu L, Zhu X, Zhang ZR, Huang Y. Novel solid lipid nanoparticle with endosomal escape function for oral delivery of insulin. *ACS Appl Mater Interfaces* 2018;**11**:9315–24.
30. Wu L, Liu M, Shan W, Zhu X, Li L, Zhang ZR, et al. Bioinspired butyrate-functionalized nanovehicles for targeted oral delivery of biomacromolecular drugs. *J Control Release* 2017;**262**:273–83.
31. Xu QG, Ensign LM, Boylan NJ, Schon A, Gong XQ, Yang JC, et al. Impact of surface polyethylene glycol (PEG) density on biodegradable nanoparticle transport in mucus *ex vivo* and distribution *in vivo*. *ACS Nano* 2015;**9**:9217–27.
32. Yang Y, Hong Y, Nam GH, Chung JH, Koh E, Kim IS. Virus-mimetic fusogenic exosomes for direct delivery of integral membrane proteins to target cell membranes. *Adv Mater* 2017;**13**:1605604.
33. Song XN, Li R, Deng HL, Li Y, Cui YN, Zhang H, et al. Receptor mediated transcytosis in biological barrier: the influence of receptor character and their ligand density on the transmembrane pathway of active-targeting nanocarriers. *Biomaterials* 2018;**180**:78–90.
34. Betker JL, Angle BM, Graner MW, Anchordoquy TJ. The potential of exosomes from cow milk for oral delivery. *J Pharm Sci* 2019;**4**:1496–505.
35. Rani P, Vashisht M, Golla N, Shandilya S, Onteru SK, Singh D. Milk miRNAs encapsulated in exosomes are stable to human digestion and permeable to intestinal barrier *in vitro*. *J Funct Foods* 2017;**34**:431–9.
36. Simbari F, McCaskill J, Coakley G, Millar M, Maizels RM, Fabrias G, et al. Plasmalogen enrichment in exosomes secreted by a nematode parasite *versus* those derived from its mouse host: implications for exosome stability and biology. *J Extracell Vesicles* 2016;**5**:30741.
37. Fan WW, Xia DN, Zhu QL, Hu L, Gan Y. Intracellular transport of nanocarriers across the intestinal epithelium. *Drug Discov Today* 2016;**5**:856–63.
38. Zheng YX, Xing LY, Chen LQ, Zhou R, Wu JW, Zhu X, et al. Tailored elasticity combined with biomimetic surface promotes nanoparticle transcytosis to overcome mucosal epithelial barrier. *Biomaterials* 2020;**262**:120323.
39. Parolini I, Federici C, Raggi C, Lugini L, Palleschi S, De Milito A, et al. Microenvironmental pH is a key factor for exosome traffic in tumor cells. *J Biol Chem* 2009;**49**:34211–22.
40. Azevedo C, Nilsen J, Grevys A, Nunes R, Andersen JT, Sarmiento B. Engineered albumin-functionalized nanoparticles for improved FcRn binding enhance oral delivery of insulin. *J Control Release* 2020;**327**:161–73.
41. Skotland T, Hessvik NP, Sandvig K, Llorente A. Exosomal lipid composition and the role of ether lipids and phosphoinositides in exosome biology. *J Lipid Res* 2019;**1**:9–18.
42. Wu L, Bai YL, Liu M, Li L, Shan W, Zhang ZR, et al. Transport mechanisms of butyrate modified nanoparticles: insight into “easy entry, hard transcytosis” of active targeting system in oral administration. *Mol Pharmaceutics* 2018;**9**:4273–83.
43. Chai G-H, Xu YK, Chen S-Q, Cheng B, Hu F-Q, You J, et al. Transport mechanisms of solid lipid nanoparticles across Caco-2 cell monolayers and their related cytotoxicology. *ACS Appl Mater Interfaces* 2016;**9**:5929–40.
44. Yang D, Liu DC, Deng HL, Zhang J, Qin MM, Yuan L, et al. Transferrin functionization elevates transcytosis of nanogranules across epithelium by triggering polarity-associated transport flow and positive cellular feedback loop. *ACS Nano* 2019;**13**:5058–76.
45. Fuentes M, Santander N, Cortes V. Insulin increases cholesterol uptake, lipid droplet content, and apolipoprotein B secretion in CaCo-2 cells by upregulating SR-BI via a PI3K, AKT, and mTOR-dependent pathway. *J Cell Biochem* 2019;**120**:1550–9.
46. Yang D, Liu DC, Qin MM, Chen BL, Song SY, Dai WB, et al. Intestinal mucin induces more endocytosis but less transcytosis of nanoparticles across enterocytes by triggering nanoclustering and strengthening the retrograde pathway. *ACS Appl Mater Interfaces* 2018;**14**:11443–56.
47. Ensign LM, Cone R, Hanes J. Oral drug delivery with polymeric nanoparticles: the gastrointestinal mucus barriers. *Adv Drug Deliv Rev* 2012;**6**:557–70.
48. Lenzini S, Bargi R, Chung G, Shin JW. Matrix mechanics and water permeation regulate extracellular vesicle transport. *Nat Nanotechnol* 2020;**15**:217–23.
49. Jeppesen DK, Fenix AM, Franklin JL, Higginbotham JN, Zhang Q, Zimmerman LJ, et al. Reassessment of exosome composition. *Cell* 2019;**2**:428–45.e418.
50. Yu MR, Xu L, Tian FL, Su Q, Zheng N, Yang YW, et al. Rapid transport of deformation-tuned nanoparticles across biological hydrogels and cellular barriers. *Nat Commun* 2018;**1**:1–11.
51. Wu L, Shan W, Zhang ZR, Huang Y. Engineering nanomaterials to overcome the mucosal barrier by modulating surface properties. *Adv Drug Deliv Rev* 2018;**124**:150–63.
52. Leroux JC. Editorial: drug delivery: too much complexity, not enough reproducibility?. *Angew Chem Int Ed Engl* 2017;**48**:15170–1.